Article

Elementary Liber Fibres Characterisation: Bias from the Noncylindricity and Morphological Evolution along the Fibre

Marie Grégoire [ID], Emmanuel De Luycker *[ID] and Pierre Ouagne [ID]

Laboratoire Génie de Production (LGP), Université de Toulouse, École Nationale des Ingénieurs de Tarbes (INP-ENIT), 65000 Tarbes, France; marie.gregoire@enit.fr (M.G.); pierre.ouagne@enit.fr (P.O.)
* Correspondence: emmanuel.de-luycker@enit.fr

Abstract: In this work, we investigate the influence of noncircularity along with cross-sectional area evolution on the measurement of the mechanical properties of elementary fibres. First, we focus on the cross-sectional area measurement and compare the circular assumption with the elliptical one using an ombroscopic device that allows the measurement of the projected diameters along the fibre as the fibre rotates around its axis, the fibre dimensional analysis system (FDAS). The results highlight important approximations to the cross-sectional area evaluation for fibres with noncircular cross sections, leading to reduced elastic modulus and stress at failure evaluated by the standard method. Additionally, results from the FDAS are used to evaluate the twist inside an individual fibre when the cross sections are sufficiently elliptical. A numerical model based on the real measured dimensions of the fibres is developed to illustrate and visualize this nonuniformity and to more accurately identify the elastic modulus. The results obtained lead us to an analytical approach that takes into account the evolution of the cross-sectional area along the fibre for a better identification of the stiffness and modulus of elasticity, which maximizes the identified mechanical properties on average by 12% for the modulus and 200% for the stress at failure. Finally, recommendations are formulated to better account for the variability along a fibre in order to evaluate the cross-sectional area.

Keywords: natural fibres; testing; mechanical properties; elementary fibres

1. Introduction

Reducing the impact of human activity on the environment is of crucial importance, and it is no longer a subject discussed only among specialists. For example, in France, the 2022 bestseller [1] by Jancovici et al. is dedicated to this topic. On the more specific subject of composite materials or technical textiles, numerous studies have investigated the interest in using plant fibres, such as flax, hemp or nettle [2–4], for example, if one wants to cite only those grown in Europe. In most of these reviews, it is generally observed that the mechanical properties of the fibres are generally very scattered. In most cases, the tensile properties of the fibres are lower than those of crystalline cellulose, which constitutes the vast majority of plant fibre cell walls. Several reasons may explain this difference. Richely et al. [5] published a paper reviewing various reasons that may explain this. They, of course, pointed to the importance of the lumen cavity, which artificially increases the surface area of the cell walls in the study of Placet et al. in [6] and in certain cases concentrates the stress applied to the fibres in these zones. It has also been hypothesized that the fibre defects, such as kink bands, created during the extraction phase [7], which reduces the working section of the fibre [8] as observed by X-ray synchrotron tomography, may also reduce the tensile properties of plant fibres and be the site of crack initiation [9–11]. Other aspects such as problems in accurately measuring the strain of fibres during a tensile test can also affect parameters, such as the elastic modulus [12]. Variable compliance of the measurement system can also affect the accuracy of the strain measurement [13]. In addition to all these aspects, the measurement of the fibre cross section, which is necessary

for the evaluation of the stress and the elastic modulus, is also a key point. There are standards [14,15] for measuring the tensile properties of bast fibres. In the standard test method, the fibre is assumed to be cylindrical, and its cross section is derived from optical microscope measurements at 3–5 locations on each fibre. However, it was shown by Garat et al. in [16] that this is not the case for technical fibres (fibre bundles). They showed that using a cylindrical model to measure the cross section of the technical fibres could lead to an underestimation of the tensile strength by 1.5. At the elementary fibre level, histological cross sections of textile flax, hemp or nettle [17–19] can show that the fibres are not cylindrical. Fibres may also show some torsion, and it is therefore difficult to determine with a high degree of accuracy the cross section to be used for evaluation of tensile parameters using optical microscopy as recommended by the standard [14]. If the fibre is not cylindrical, it may show its small or large apparent diameter, and 3–5 measurements per fibre may not be sufficient to determine an optimal mean value. In this work, it is proposed to investigate some of the systematic errors that may occur during the traditional evaluation of the fibre cross section and to study some of the possibilities offered by the use of a shadow projection device. In particular, it is proposed to study, as for fibre bundles [16], the interest of using an elliptical model to determine the fibre cross section. The study will even go beyond by investigating the evolution of the fibre morphology (ellipticity level, fibre twist, and cross-section variations) on the property evaluation.

2. Materials and Methods

2.1. Material—Measured Fibres

The tests were carried out on several materials in order to highlight the influence of the type of fibre on the results obtained. First, textile flax (*Linum Usitatissimum* L.) of the Bolshoi variety grown in Normandy was dew-retted for 3 weeks before being harvested and baled with oriented stalks. The fibres used in this study were extracted from these stalks using a laboratory scale scutching/hackling apparatus consisting of three separate modules: breaking, scutching, and hackling. Oilseed flax (*Linum Usitatissimum* L.) of the Everest variety was grown in Southwestern France by Ovalie Innovation (Auch, France). The material was harvested and baled immediately after seed maturity in early July. Fibres were then extracted using a Laroche Cadette 1000 full-fibre extraction unit. The hemp (*Cannabis sativa*) fibres studied were obtained from the upper parts of male stems of the Carmagnola variety. These were retted for 3 weeks before the fibres were extracted using a scutching/hackling device similar to that used for flax fibres. The last batch corresponds to stinging nettle (*Urtica dioica*) fibres manually extracted from hand-harvested stems. Prior to extraction, the stalks were immersed in water at room temperature for 24 h to facilitate fibre separation.

2.2. Sample Preparation for Optical Microscope Cross-Section Observation

In addition to the abundant literature on hemp and textile flax microscopic observations, cross-sectional observations (Figure 1) were made on oilseed flax fibres to visualize their shape.
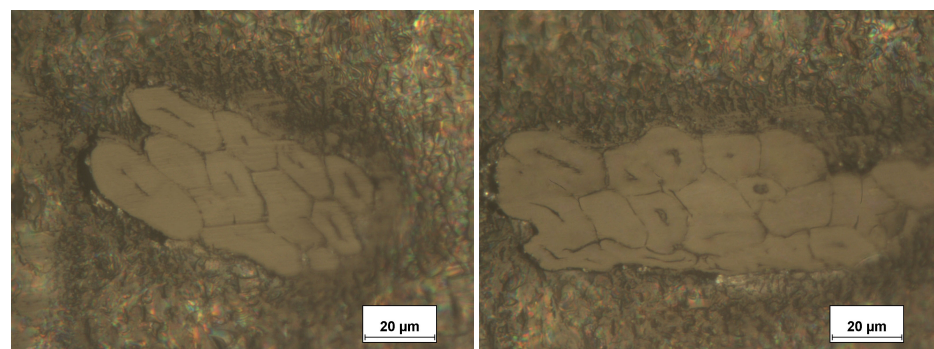

Figure 1. Oilseed flax bundles of fibre.

For this purpose, fibre bundles were collected from the output of the Laroche Cadette all-fibre device before being positioned vertically in a bucket filled with a coating matrix. In this research, the sample was fabricated by cold mounting. After curing for 5 min, the assembly was removed from the mold and allowed to air dry for at least half a day. Sections were then cut on a microtome with a tungsten blade. Twenty micrometer slices were cut in each pass. After cutting, the sample was polished in three steps. First, a quick polish with 1000 grit paper was performed to roughly remove any striations that may be present on the surface of the sample after cutting. Two further polishing steps were performed with 6 μm and 4 μm paste, respectively, until a sufficiently clean surface was obtained to observe the fibres under the microscope. Each polishing step was followed by the immersion of the specimen in an ultrasonic bath to remove any polishing particles that may interfere with observation of the fibres.

2.3. Optical Microscope—Axial Observations of Fibre Cross Sections

Following the methodology described in the previous section, the actual cross-section area of eight oilseed flax fibres was plotted and measured (Figure 2) using ImageJ image processing software developed by the National Institutes of Health (NIH) (ImageJ, Bethesda, MD, USA). The minimum and maximum widths of each of these fibres were also recorded.
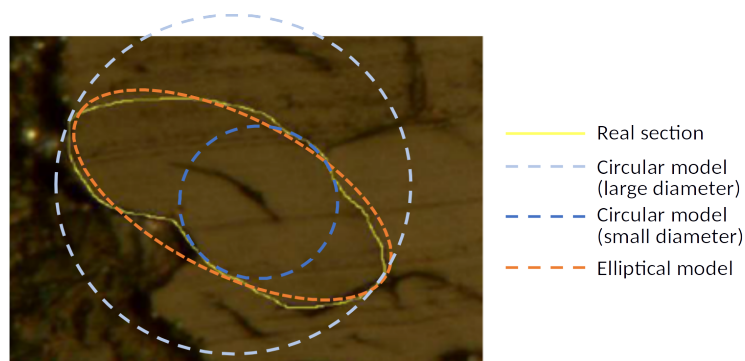

Figure 2. Considered models to represent the cross section of a natural fibre.

2.4. Optical Microscope—Transverse Uni and Bi-Directional Cross-Section Measurement

As stated in the NF T25-501-2 standard [14], the fibres were glued onto paper frames (Figure 3b) with a gauge length of 12 mm before being sized using a light microscope (Olympus PMG3-F3, France) at a magnification of ×40 to determine their apparent diameters (see Figure 3a). Observations at 0° angle (as defined in Figure 3b) were made on 30 oilseed flax fibres and 30 textile flax fibres. Nine measurements were taken along the length of each fibre, and the values obtained were averaged according to the standard.
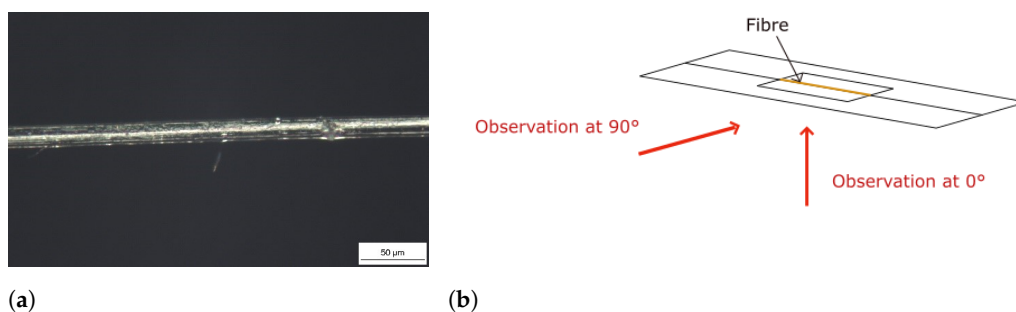

(**a**)   (**b**)

Figure 3. Optical microscope cross-section measurement. (**a**) Observation of a textile flax fibre with a magnification of ×40 and (**b**) fibre mounted on a paper frame for observations at 0° and 90°.

To complement the standard approach, an observation at 90° (as defined in Figure 3b) was made. Technically, paper frames were bent at 90°, and the same microscope was used

to obtain the image. As in the standard, nine measurements distributed over the gauge length were also made in this second direction of observation and averaged.

2.5. Dia-Stron Ltd FDAS—Multi-Directional Cross-Section Measurement

To go further in the knowledge of fibre-section areas (for a finer processing of tensile testing results), an ombroscopic dimensioning device was used. This is the fibre dimensional analysis system (FDAS) (see Figure 4a) controlled by UV Win software and developed by Dia-Stron (Diastron Ltd., Hampshire, UK). The fibre to be dimensioned is mounted on plastic tabs using a UV curable adhesive (DYMAX, Wiesbaden, Germany) and also a gauge length of 12 mm. The assembly is then positioned in the rotating jaws of the device and held in position by a pneumatic system.
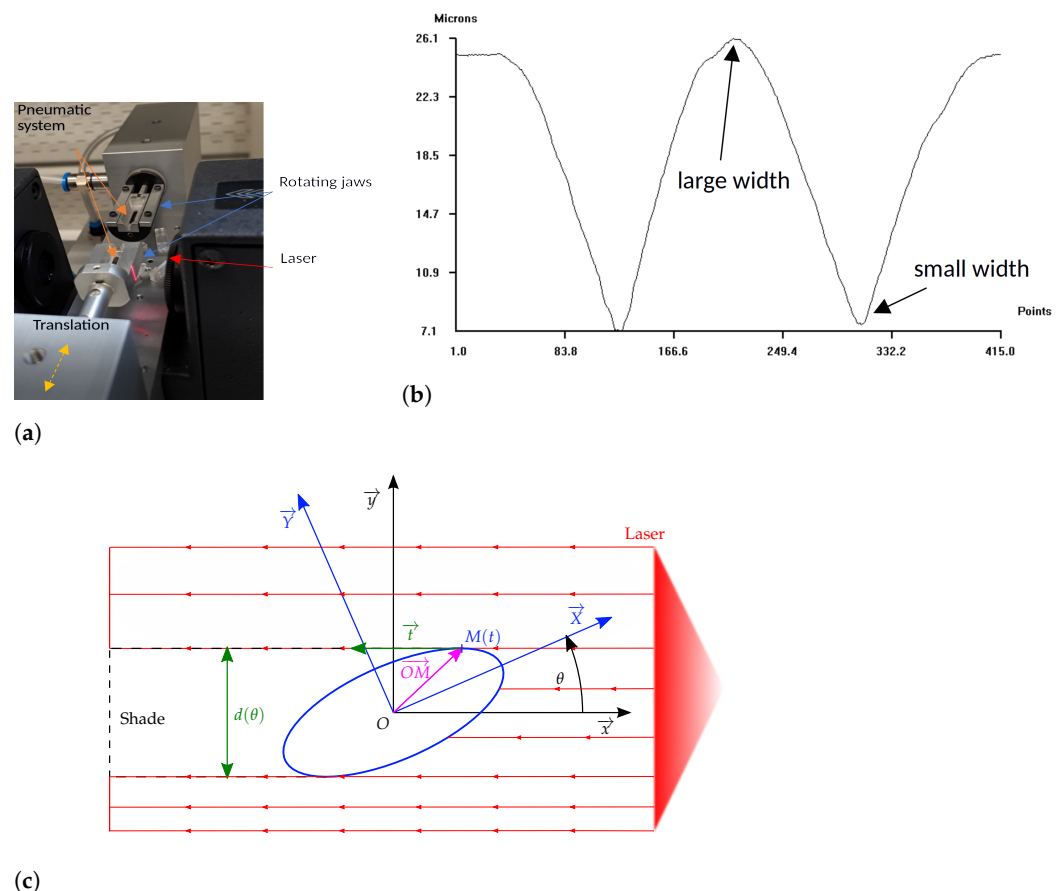

(a)

(b)

(c)

Figure 4. (**a**) Fibre dimensional analysis system (FDAS) developed by Dia-Stron; (**b**) evolution of the projected diameter of an oilseed flax fibre during a full rotation for a given slice along the fibre; (**c**) projected diameter *d* of an elliptical fibre for a given angle θ.

The projected diameter of the fibre was measured using a high-precision laser (LSM 500S, Mitutoyo, Japan). A full rotation of the fibre around its axes allows recording all projected diameters Figure 4b as the θ angle Figure 4c evolves. After a small translation in the fibre direction, this operation was repeated for each section (up to 74 times) along the fibre length, giving the evolution of the projected diameter along the fibre. Minimum and maximum projected diameters were recorded for each measured section. The projected diameters were measured with the accuracy of 0.01 μm.

2.6. Measurement of Twist

For elliptical fibres (with a low circularity index (defined as the ratio of the small width to the large width)), an angle can be defined between the major axis of the section (approximated by an ellipse) and a reference. The natural twist of each fibre is then

evaluated. Assuming a constant rotational speed and the same angular position at the beginning of each slice measurement, the phase shift that occurs in the projected diameter evolution between two successive slices is related to the amount of twist inside the fibre. To evaluate this twist, we compared the position of the maximum and minimum projected diameter during the measurement of each slice as shown in Figure 4b with a reference position (slice 1).

With the selected settings, a projected diameter was recorded for each degree of rotation of the instrument. This was confirmed by measuring the distances between two peaks representing half a rotation of the fibre. Data processing was performed using the open-source software Octave [20].

The methodology was validated by gradually introducing an artificial amount of twist on the same fibre on the FDAS instrument. Figure 5 shows the twist evolution along the fibre (slice 1 corresponds to the clamped side of the fibre and slice 74 to the side where the rotation is applied after two scans at a given twist level). The slope of these curves is directly related to the twist unit angle. The same fibre was scanned twice for each imposed twist level to evaluate the repeatability of the method. The level of twist increased gradually and the same fibre was scanned twice with no introduced twist (curves ref_1 and ref_2) and then after adding 2 turns to the reference ($ref + 2turns_1$ and $ref + 2turns_2$), 4 turns ($ref + 4turns_1$ and $ref + 4turns_2$), 7 turns ($ref + 7turns_1$ and $ref + 7turns_2$), 9 turns ($ref + 9turns_1$ and $ref + 9turns_2$) and 19 turns ($ref + 19turns_1$ and $ref + 19turns_2$). Note the intervals between the curves for the 74th section, which clearly confirms the ability of the method to evaluate the torsion of a fibre as long as its section is sufficiently elongated.
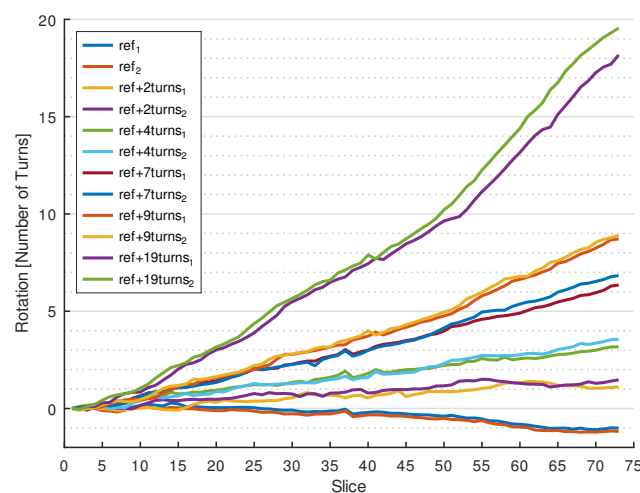

Figure 5. Twist measurement verification on the same fibre with 0 turns, 2 turns, 4 turns, 7 turns, 9 turns and 19 turns—each scan is performed twice, slice 1 corresponds to the clamped side, and slice 74 corresponds to the side rotating between the scans.

2.7. Elementary Fibre Tensile Test Using LEX820 Device

Following section and twist measurement using the FDAS device, the fibres were tested in tension to determine their mechanical properties. The used device is a high-precision extensometer LEX820 (Dia-Stron Ltd., Hampshire, UK) developed specifically for testing natural fibres. It consists of a stepper motor that controls the displacement with the accuracy of 1 μm associated to a load cell with a capacity of ±20 N. The device is suitable for materials that break at a low level of deformation and low load. The tests were performed at a displacement speed of 1 mm/min and a sampling period of 20 ms. When a drop in the load level of more than 0.05 N was observed, the test was stopped. A more detailed presentation of this device can be found in [16,21].

After mechanical testing, an average section considering either a circular or an elliptical section was calculated from the measurement data in order to identify the stress at failure

and the elastic modulus. This later one was evaluated depending on the behaviour type—I, II or III—of the fibre [6,22–25] on the initial slope, the global slope, or the slope just before failure.

2.8. Isogeometric Numerical Model of the fibre

The projected diameters (minimum and maximum) and twist were used to reconstruct an elliptical cross section of each slice with its orientation angle. This can be repeated for all the 74 considered sections. Although an exact reconstruction of the fibre cross section is not possible (nonconvexities remain hidden when using an ombroscopic measurement apparatus), a global view with the evolution of sections and twist can be performed. Considering the evolution of large- and small-axis dimensions together with the orientation angle along the fibre, a polynomial fit (degree 5 is chosen) was extracted based on the data from the 74 sections in order to automatically reconstruct the 3D mesh for the simulation. An example of section evolution is presented later in Section 3.4 for a few bast fibres. An elliptical assumption was made for the cross section, and the geometry was represented using an isogeometrical mesh [26] for the simulation. The choice for this method was made based on the fact that elliptical cross sections can be represented exactly with only one element with quadratic NURBS shape functions associated with nine control points. The material model used was elastic and isotropic driven by a Young modulus E and a Poisson ratio ν. This later coefficient is difficult to evaluate and will be considered equal to 0.498 in this work as identified by [27] using an inverse method on a flax epoxy composite.

2.9. Identification of the Modulus from Simulation and Analytically

Tensile data are exploited here in order to identify with more accuracy the elastic modulus. The fundamental hypothesis made is the homogeneity of the material constituting the fibre and that the lumen is considered negligible (fully filled fibres). Dia-Stron software considers a mean section in order to compute a stress from the measured load.

Two sources of improvement are raised in this work considering the stress at failure or the elastic modulus:

- In terms of stress at failure, the concept of an average section is not necessarily the most appropriate, considering the fact that, at failure, the smallest section exhibits a higher stress than a mean section. This is illustrated in Figure 6, where the colour represents the level of von Mises stress, which is obviously not constant along a fibre since the section area evolves.

  Assuming again that the material exhibit a similar behaviour at failure along the fibre, the failure is likely to occur in the smallest section, where the stresses are maximal. For evaluating the stress at failure, we recommend using the smallest section along the fibre instead of a mean section.

- In terms of the elastic modulus, considering the assumption of a mean section S_m in Dia-Stron software, an elastic modulus E_m is identified based on Formula (1):

$$E_m = \frac{F/S_m}{\Delta L/L} = \frac{F\,L}{S_m\,\Delta L} \tag{1}$$

The total stiffness of a fibre is the combination of all the local stiffness along the fibre (such as springs put in series) since the total elongation is the sum of all the local elongations. The numerical model proposed in Section 2.8 with varying sections (Figure 6) naturally takes this aspect into account. From a practical point of view, the fibre modulus is identified by the inverse approach, taking an experimental extension of the fibre and adjusting the elastic modulus on the model in order to obtain a resulting tension in the fibre corresponding to the load measured experimentally. Alternatively, if we neglect the geometric nonlinearity and consider a constant stress within a given section, as soon as the evolution of the section is known along the fibre, a similar identification can be performed considering the 1D integral (Equation (4)). This equation is obtained assuming that the total elongation of the fibre comes from

the local strains, which are considered depending on the local section of the fibre (Equation (2)) (constant stress within the section):

$$E = \frac{\sigma(x)}{\varepsilon(x)} = \frac{F/S(x)}{du(x)/dx} \quad => \quad \frac{du(x)}{dx} = \frac{F}{E\,S(x)} \tag{2}$$

$$\Delta L = \int_0^L du = \int_0^L \frac{du(x)}{dx}dx = \frac{F}{E}\int_0^L \frac{dx}{S(x)} \tag{3}$$

$$E = \frac{F}{\Delta L}\int_0^L \frac{dx}{S(x)} = \frac{E_m\,S_m}{L}\int_0^L \frac{dx}{S(x)} \tag{4}$$

In a discreet manner, considering a number n_{sec} of sections equally distributed of Δx along the fibre (similar to what we face on the scanning device with a discrete number of slices), Equation (4) can be rewritten as Equation (6), introducing the average section $S_m = 1/n_{sec}\sum S_i$ and average of the inverse of the sections $(1/S)_m = 1/n_{sec}\sum 1/S_i$ and considering the fact that $L = n_{sec}\Delta x$:

$$E \approx \frac{F}{\Delta L}\sum_{i=1}^{n_{sec}}\frac{\Delta x}{S_i} = \frac{F\,n_{sec}\Delta x}{n_{sec}\,\Delta L}\sum_{i=1}^{n_{sec}}\frac{1}{S_i} = \frac{F\,L}{\Delta L}\left(\frac{1}{S}\right)_m \tag{5}$$

$$= E_m\sum_{i=1}^{n_{sec}}S_i\sum_{i=1}^{n_{sec}}\frac{1}{S_i} = E_m\,S_m\left(\frac{1}{S}\right)_m \tag{6}$$

The coefficient $K_E = S_m \times (1/S)_m$ (discussed Section 3.6) illustrates the ratio between the real modulus for a fibre with an evolving section, and the approximated modulus, taking into account an average section during identification.
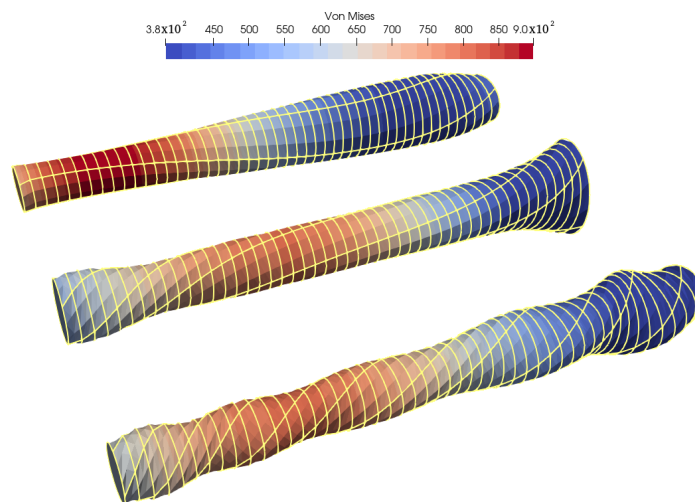

Figure 6. The tensile test simulation of a fibre with varying elliptical section and an increased torsion: reference fibre (**top**) is tested again after 3 turns (**middle**) and 8 turns (**bottom**) (for representation purpose, due to the extreme aspect ratio of individual fibres, the scale in the section is magnified $\times100$).

2.10. Statistical Analysis

Tests, known as two-sample t-tests, were carried out to check whether a significant difference could be observed between the mean values of the two batches. A confidence interval of 95% was taken into account.

3. Results

3.1. Influence of the Chosen Calculation Method on the Section Area of an Individual Fibre and Comparison with the Real Section

The cross-section area of an elementary fibre must be measured accurately in order to limit significant variations in mechanical properties. The ASTM D3822/D3822M-14 [15] and NF T25-501-2 [14] standards assume that bast fibres are cylindrical and that measuring a width using an optical microscope in a single orientation is sufficient to perform the calculation of a cross-section area that is close to the real area of the individual fibre [14,21]. In the case of synthetic fibres with controlled cross sections, this assumption can be applied with good confidence, but it may not be the same for natural fibres, where the cross sections along the fibre are not homogeneous [28,29]. Cross sections were measured on oilseed flax fibre bundles images with the objective to determine if a circular model can be considered to measure a single fibre cross-section area. The results obtained are presented in Figure 1.

The results on oilseed flax fibres show that, at the locations where the cross sections were measured, many fibres have elongated shapes that are closer to the elliptical than to circular sections. This was already shown on elementary flax and sisal fibres by Thomason and Carruthers [30] and on bundles of textile flax, hemp, nettle, sisal and palm by [16]. Cross sections from the literature on textile flax, hemp or nettle fibres [17–19] also show that this noncircularity of the cross sections of individual fibres can be found in materials other than oilseed flax (see Figure 7).
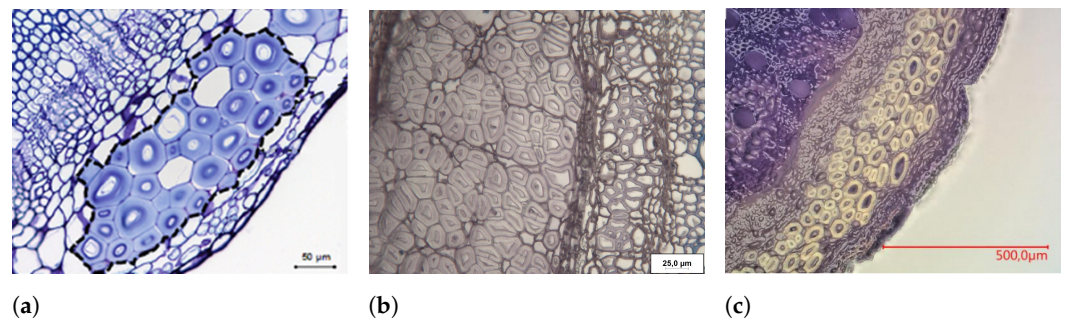

(**a**)   (**b**)   (**c**)

Figure 7. Cross sections of stems. (**a**) Textile flax [17]; (**b**) hemp; (**c**) nettle [19].

In order to quantify the impact of the model chosen to evaluate the cross section of an individual fibre, the actual cross sections of several fibres of the bundles shown in the cross sections of Figure 2 were measured on the ImageJ software, and the results were compared with the cross sections calculated according to circular or elliptical models from the minimum and maximum widths obtained on the image processing software. Several types of circular models were studied. Indeed, if the observation of the fibres is carried out by optical microscopy as required in the standards, only one width value can be recorded at a time, and the cross-section area using the circular model is only calculated according to the type of width that is possible to observe. Figure 2 shows what approximated sections can be obtained depending on the type of geometrical model followed.

The results obtained from the geometrical models presented Figure 2 on eight fibre sections are presented in Table 1.

Table 1. Measurement of the actual cross section of oilseed flax fibres according to different models.

	Real Measured Area (µm²)	Difference (%)/Measured Area ImageJ			
		Elliptical Model	Circular Model (Large Diameter)	Circular Model (Small Diameter)	Circular Model (Mean Diameter)
Mean	163	+2	+129	−48	+21
Standard-deviation	110	5	120	16	26

They show, first of all, that the elliptical model gives a section area value very close to the real value measured with the ImageJ software. The different circular models generate very large errors, up to more than 100%, when the fibres are not perfectly circular, with a dramatic impact on the identified mechanical properties. Thus, if the optical microscopy observation is carried out when the fibre is positioned at its widest point, this would lead to a strong overestimation of the area of the fibre and therefore an underestimation of its real mechanical properties. Conversely, if the value measured under microscopy corresponds to the smallest width of the fibre, this would lead to an underestimation of its area and therefore to an overestimation of its mechanical performance.

3.2. The Impact of the Use of Optical Microscopy on the Cross-Sectional Measurements of Individual Fibres

It is important to know which width (large or small) of the fibre is measured when it is observed under the optical microscope. As shown in Section 3.1, this has an effect on the over- or underestimation of the fibre cross sections and thus on the calculated mechanical properties. For this purpose, 100 fibres from the same batch of textile flax and oilseed flax were observed by optical microscopy at 0° and 90°, where 0° is the position when the fibre and its paper frame are laid flat on the optical microscope. The results of the tests on textile flax show that 73% of the fibres had a larger diameter when the frame was placed at 0° than when it was placed at 90°. This percentage is even higher for oilseed flax, where the percentage rises to 79%. Thus, the vast majority of the fibres are positioned at their widest width when glued to the paper frames as recommended by the standard. This method of preparation and measurement by optical microscopy therefore introduces a systematic error due to the natural positioning of the fibres when they are glued. In the vast majority of cases, the area of these fibres is therefore calculated from the largest width of the fibre, which leads to an overestimation of about 130% of the cross-sectional areas and thus to a general underestimation of the mechanical properties of the plant fibres.

3.3. Measurement of Apparent Widths by the FDAS System

The oilseed and textile flax fibres observed under optical microscopy are also scanned in the same orientation on the FDAS device. The latter measures the apparent diameters of the fibres recorded around their entire circumference Figure 4b and at several points along the gauge length. A sample of the data recorded is presented Figure 8 and illustrates the evolution along the fibres of the section (projected diameter level) and also the circularity (boxplot height).
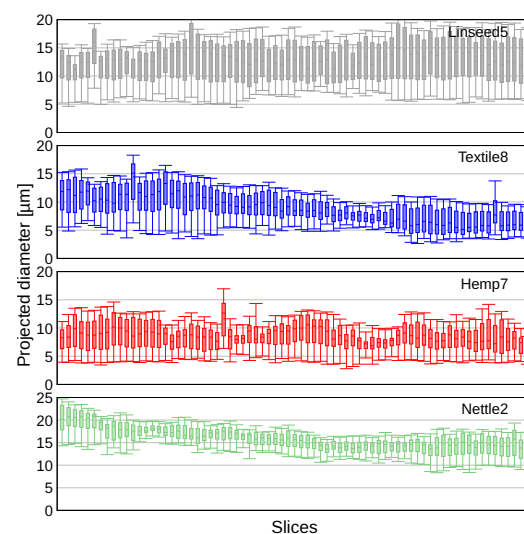

Figure 8. Projected diameter boxplot per slice along the length of linseed flax, textile flax hemp and nettle fibres (scale for nettle is different from other fibres).

The small and large widths of each fibre are recorded and can be used to calculate fibre cross sections using the desired model (elliptical or circular). The results obtained show that the high-precision laser registers strong variations in apparent widths at the same position when the fibre is rotating around its axis. An example of a measurement on a slice of an individual oilseed flax fibre is shown in Figure 4b. In this case, it can be seen that at the same position along the fibre, the widths vary from 7.1 µm to 26.1 µm. This large variation is observed at different positions on all the gauge lengths of the tested fibres but with variations of amplitudes that can be different.

On fibres measured from our data on oilseed and textile flax, textile flax presents a greater width of 107% compared to its smallest width, whereas this percentage rises to 116% for oilseed flax.

Geometrically, the fibres being elliptical and the rotation of the fibre being with a constant angular speed during the FDAS measurement, a number of widths larger than the arithmetic mean value between the minimum and maximum width measurement is expected to be measured. The tests were performed on oilseed and textile flax, hemp and nettle fibres. It appears that 57% of nettle, 61% of hemp, 63% of textile flax and 68% oilseed flax positions recorded by the FDAS are above the width arithmetic value. This clearly means that the fibres during their rotation show more width above the mean value.

It also appears that oilseed flax fibres are statistically more elliptical than textile flax, hemp and nettle fibres, respectively, in our case. This is also confirmed by the calculation of the circularity index (small width to large width ratio) and their statistical distribution for each tested type of fibre (Figure 9).
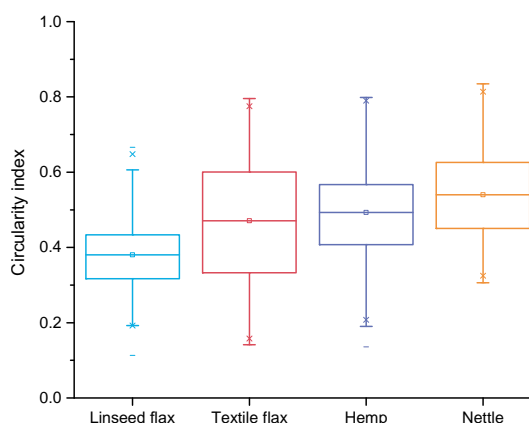

Figure 9. Circularity index distributions (small to large width ratio) for different types of fibres.

Although all materials are highly elliptical, textile flax has an average circularity index of 0.51, while that of oilseed flax is 0.39. This high ellipticity means that using a circular model would result in large differences from the actual fibre area.

Table 2 shows the difference observed according to the calculation models used (elliptical or circular) when measuring average sections on the same fibre with the FDAS system. The elliptical model is calculated from the small and large widths, while the circular model is calculated from an average between these two values. A comparison is made with the measurement made on the same fibres with an optical microscope.

Table 2. Calculation of fibre cross sections according to the model (circular or elliptical) used.

	Average Section Elliptical Model (µm²)	Difference (%)/Elliptical Model	
		Average Section Circular Model FDAS	Average Section Circular Model Microscopy
Linseed flax	150.6	+31	+55
Textile flax	73.8	+16	+46

It appears from Table 2 that the use of a circular model from the FDAS (which takes an average diameter on all the different measured positions) data results in an overestimation of the average cross-sectional area by 31% and 16%, respectively, for oilseed flax and textile flax fibres, compared to the cross-sectional area calculated with an elliptical model. The difference in results between the two materials can be explained by their level of ellipticity. It was shown previously that oilseed flax fibres have a more elliptical cross section than textile flax fibres. Oilseed flax fibres show a greater difference between their minimum and maximum widths, which has a direct impact on the calculation of cross sections with a circular model. When the cross-sectional calculations are carried out using the microscopy data and a circular model, the difference in measured cross section increases to 55% for oilseed flax and 46% for textile flax. The systematic measurement error due to the fact that the fibres lie on their large side in almost 80% of cases is visible here. The values obtained are lower than what was observed in Section 3.1 when the cross sections were calculated from cross sections. This is mainly due to the fact that, when glued to the paper frames, the fibres do not lie completely flat but rather in an intermediate position as shown on the right in the Figure 10. It should also be noticed that the FDAS sizing device used in this study does not allow for the measurement of concave areas, which can also lead to measurement approximations in some particular cases.
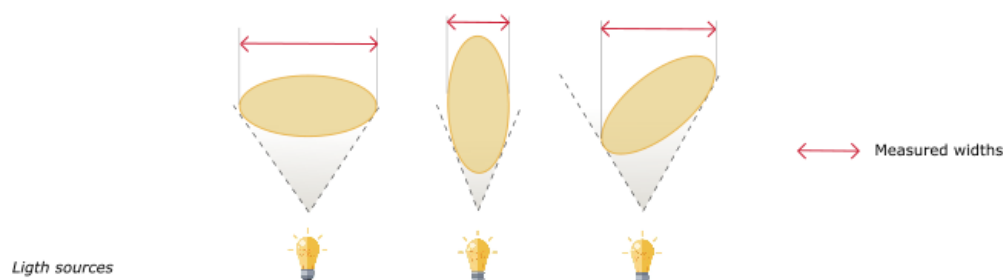

Figure 10. Orientation possibilities of an elliptical fibre when measured by optical microscopy.

The use of a circular model on fibres measured by optical microscopy therefore leads to an overestimation of the fibre cross section by about 50%. This results in a 50% drop in stresses at the break and elastic moduli. This means that in many of the studies available in the literature to date, the tensile properties of elementary plant fibres are underestimated. The correction factor that should be applied is, however, difficult to define precisely since it depends on the circularity rate of the fibre studied. Indeed, the results presented in Table 2 show that for an oleaginous flax fibre with a circularity rate lower than 50%, the error is more important than for a textile flax fibre with a less severe noncircularity. Thus, if the elementary fibres have circularity indices below 0.8, it is necessary to use an elliptical model instead of a circular one. However, it appears that for the vast majority of hemp, oilseed flax and, to a lesser extent, textile flax fibres, the indices are practically all below this limit. The use of an FDAS-type device to measure fibre sections may therefore be a solution for limiting errors by using an elliptical model. It might be worthwhile to modify the test standard in this direction.

3.4. Fibre Section Area and Circularity Evolution along Their Lengths

It was shown in Section 3.2 that oilseed flax and textile flax fibres have circularity indices globally lower than 0.5, illustrating a pronounced ellipticity of the sections. The study of the evolution of this index (within different slices) along the fibres observed previously on the FDAS device shows that the fibres do not have a uniform section along their length (see Figure 11).
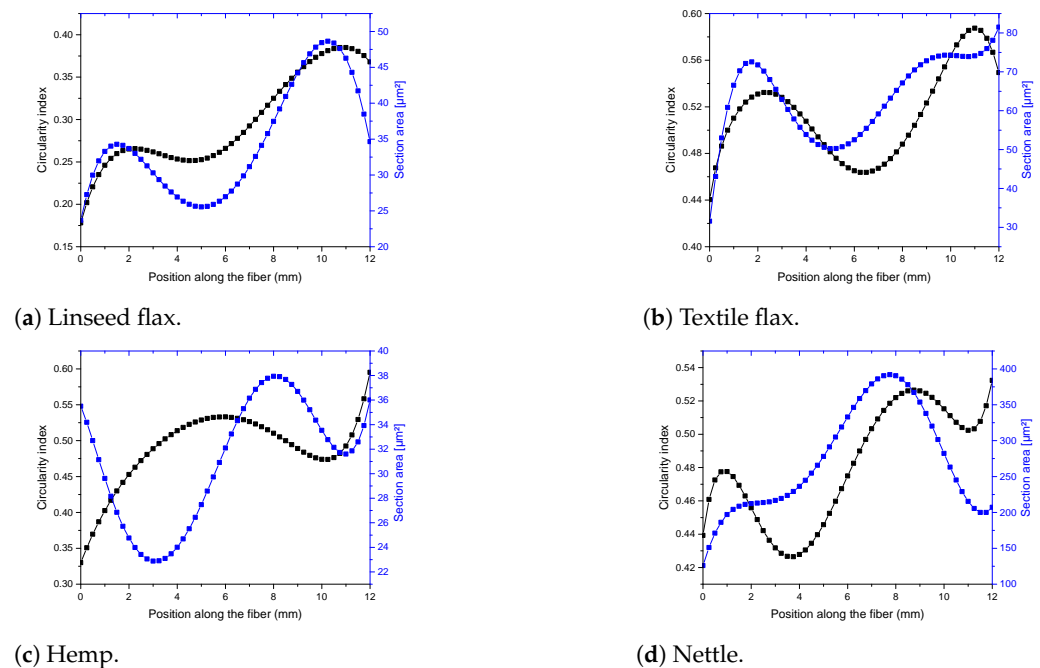
(**a**) Linseed flax.

(**b**) Textile flax.

(**c**) Hemp.

(**d**) Nettle.

Figure 11. Fibre section area and circularity index evolution along the fibre length (degree 5 polynomial fit) for different bast fibre plants.

In order to quantify this evolution more precisely, fibres of textile flax, oilseed flax, hemp and nettle were scanned more accurately (74 measurements over the gauge length) on the FDAS device. The evolution of the measured section area and circularity index along the fibres are presented in Figure 11 for a sample of fibres. Both the section area and circularity index are far from being uniform for a given fibre with a circularity index ranging from 0.42 to 0.53 for the most uniform (nettle Figure 11d) fibre and section area from 23 μm^2 to 38 μm^2 for the most uniform (hemp Figure 11c) fibre.

3.5. Natural Twist

Using the FDAS measurement tool, the natural twist of several fibres of different types was evaluated according to the method described in Section 2.6. The results, presented in Figure 12, show the important level of torsion encountered in most fibres; these results are also used when building the geometric model used for the 3D simulation.

The measured levels of torsion could be some sources of nonlinearity that need to be further investigated. If most of the fibres show a monotonous evolution of the twist, some fibres, on the contrary, have a twist level that increases before decreasing (or vice versa), indicating a change from clockwise to counterclockwise (or vice versa) within a given fibre. Naturally, levels in the range of 2 to 5 turns were commonly measured.

From those curves, a maximum unit torsion was evaluated (keeping only the maximum rotation together with the location of this maximum along the fibre) and a distribution of those maximum twists is presented Figure 13.

Conclusions are that on 12 mm, all fibres present more than one turn and that a sample of width measurements with the standard approach should include large and small widths (or major and minor axis with an elliptical assumption) of the section. Revisions to the standards could recommend keeping the maximum and minimum measured widths to calculate an elliptical section area rather than averaging those widths with a circular model. This would only apply to fibres that are sufficiently regular along their length.
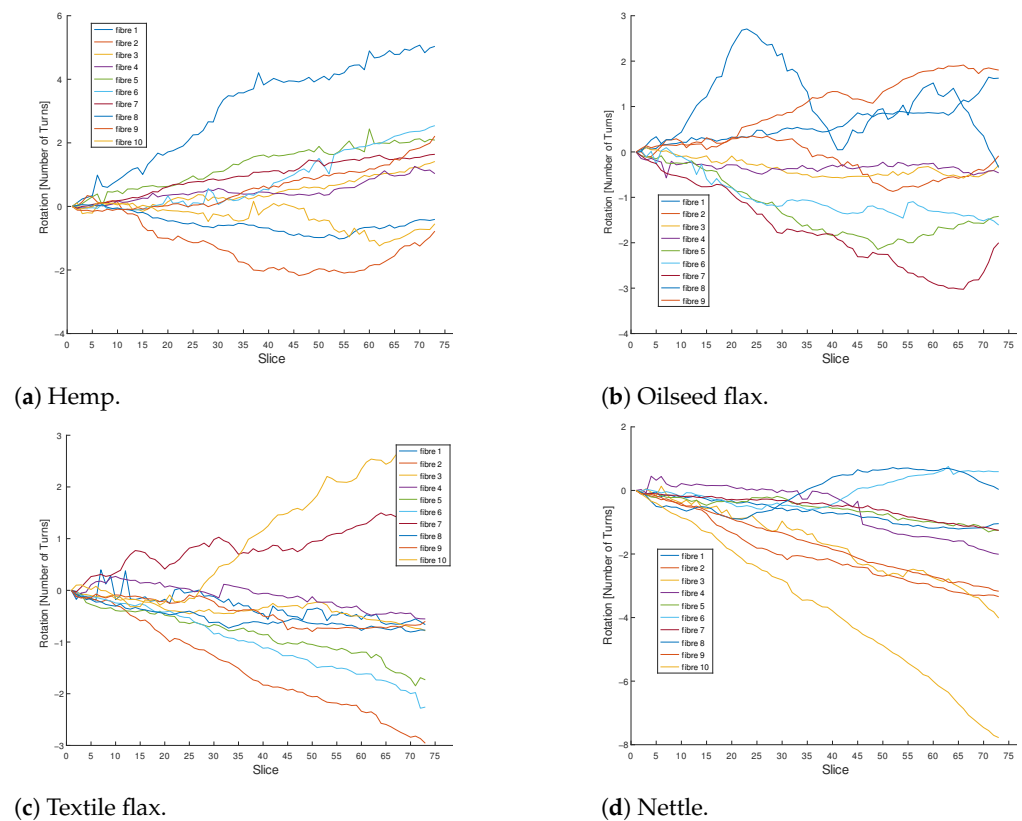
(**a**) Hemp.

(**b**) Oilseed flax.

(**c**) Textile flax.

(**d**) Nettle.

Figure 12. Natural twist for different types of fibres—rotation of each slice along the fibre.
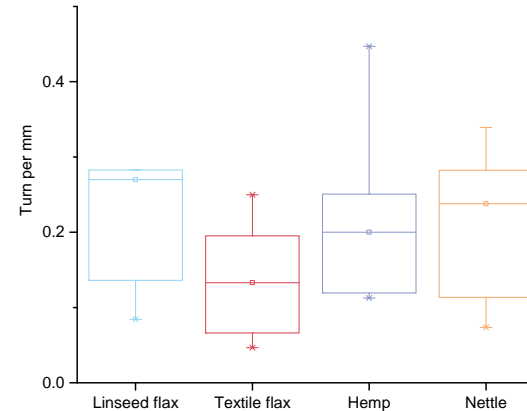

Figure 13. Torsion distributions for different types of fibres.

3.6. Elastic Modulus and Stress at Failure

Using the method described in Section 2.8, an image of a reconstructed fibre is proposed in Figure 6. The fibre represented is the same hemp fibre, with its natural twist on top, three additional turns for the middle one, and eight turns for the bottom one. The variation of twist as well as the variation of the section are clearly visible. On places where the sections are minimal, the evaluated von Mises stress is higher. This suggests that the fibre failure during a tensile test has more chances to take place in such a place and, of course, the local stress is expected to be higher than if a mean section value is taken into account. This means that if one assumes that the fibre does not contain any defect, such as kink-band [31], the real value of the failure stress is higher than what is given following the experimental test using FDAS associated with an elliptical mean section and even higher than if the section is measured using a circular model determined under an optical microscope. The stress at failure should be calculated with the minimum section present in the fibre. Two coefficients are considered and plotted in Figure 14:

- K_E, defined in Section 2.8, represents the gain in terms of identified elastic modulus between the average elliptical section and the model with varying section.
- K_r represents the ratio between the average section and the minimal section, which is also the expected gain in terms of stress at failure.
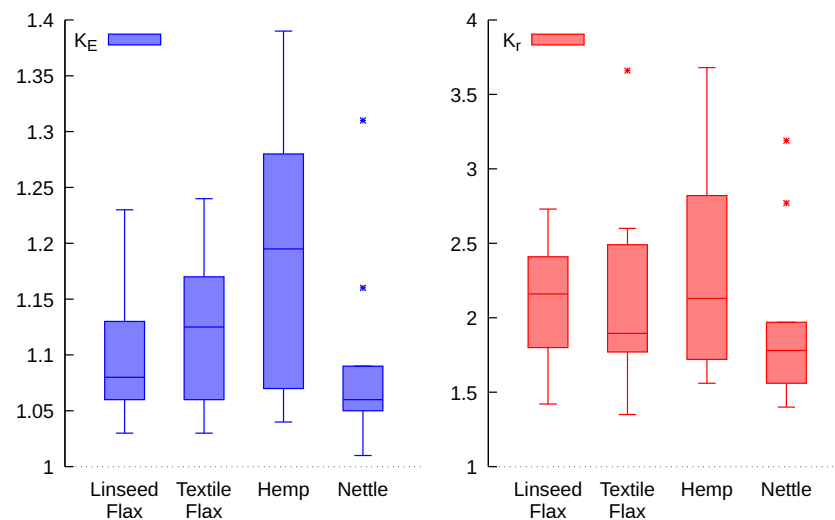

Figure 14. Increase coefficients for elastic modulus K_E on the left and stress at failure K_r on the right for all fibre types.

Regarding the data, nettle is little impacted by K_E due to little section evolution along the fibre length. Hemp is the most impacted both in terms of elastic modulus and stress at failure. The K_E maximum value is 1.39, which corresponds to an increase of 39% of the elastic modulus. The average value of K_E is 1.12, leading to an average increase of 12%. In terms of stress at failure, the K_r coefficient is much greater with a maximum value at 3.68 for hemp, and median values are close to 2, indicating that the stress at failure identified at the smallest cross-section zone is doubled in comparison to the mean value.

4. Discussion

Considering the various results presented in this paper, classical standards fail to properly represent the mechanical properties of natural fibres in the following cases:

- Circularity is not high enough;
- The cross-sectional area varies greatly along the fibre.

The area evaluation is of primary importance for the ultimate strain evaluation. An elliptical description of the cross section is mandatory to reduce the area approximation as identified in Table 1. In this context, and assuming that the fibre section evolves little along the fibre, instead of a mean diameter calculated from the average of the 10 projected diameters, one could identify an elliptical equivalent section, whose dimensions are the minimum measured projected diameter for the minor axis and the maximum measured projected diameter for the major axis as shown in Figure 10.

Considering that the cross section evolves along the fibre, the only way to capture this aspect is to use scanning devices capable of measuring the fibre cross-section evolution, such as an FDAS system.

The variation of the cross section is particularly important when evaluating the stress at failure, as large variations in cross-sectional area were observed. Variations in the cross-sectional area of a factor of 2 were observed, indicating an increase in local stress. This means that the plant fibres tested in this work can sustain much higher stresses than those determined using any type of average cross-sectional value. The true ultimate strength of the fibre should be considered at the smallest cross section. This consideration is only valid if the internal voids and defects, such as kink bands, are neglected. The global stiffness of a

fibre is the result of all the sections added in series, which requires a numerical simulation for the inverse identification of Young's modulus, or, once the evolution of the section along the fibre is known, Equation (6) allows taking into account the evolving section of the fibre. By considering this approach, it was observed that the stiffness of the fibre is improved by up to 39% for hemp fibres (12% on average) and by a few percentage points for the other fibres. This shows that it is very important to evaluate the cross section of the fibres all along their length, as it drastically improves the evaluation of the tensile strength and, by a few percent points, that of the fibre stiffness.

5. Conclusions

The work presented in this study aims to improve the evaluation of the tensile properties of bast fibres, such as flax, hemp or nettle. It concentrates on the determination of fibre cross sections necessary to compute parameters, such as the stress or the elastic modulus. It is demonstrated that the methodology described in the standard test methods widely underestimates the values of the fibre properties due to systematic measurement errors in the fibre cross section. The use of shadow projection to evaluate the cross section of the fibre by using an elliptic model from the mean lower and larger projected diameters greatly improves the results. However, the fibre reconstructions presented in this work also demonstrate that the cross section of the fibre varies along its length. Large variations may be observed. In this case, the ultimate failure stress should be computed at the smallest section area location if one assumes that the fibre contains no defects. With this assumption, it is observed that the failure stress can be doubled in comparison to the approach using a mean cross-section value, even when evaluated using an elliptical model. Higher elastic moduli (about 10% increase) are also determined when considering a fibre with variable cross-section portions. These results are obtained on a limited number of fibres, which probably justifies the fact that a large dispersion is observed (especially for hemp). New campaigns carried out on a larger number of batches and on a larger number of fibres per batch would reinforce the precision of the results obtained in this work and confirm or disprove the trends observed between different species.

The results presented in this work therefore contribute to the improvement of the fibre property evaluation and to understanding why the properties evaluated experimentally are far from the ones expected for a structure mainly constituted from crystalline cellulose. In a future work, it would be interesting to combine the approach proposed in this work (using a systematic reconstruction of the fibre cross section using an elliptical model) with a study of the effect of internal defects (kink bands) present in natural fibres. The combination of both geometric and defect approaches would open the possibility to more accurately evaluate the ultimate stress and elastic moduli of natural fibres and to adjust the total amount attributed to internal defects versus geometric variability, which has probably been overestimated so far.

Author Contributions: Conceptualization, E.D.L. and P.O.; methodology, M.G. and E.D.L.; formal analysis, M.G. E.D.L. and P.O.; investigation, M.G. and E.D.L.; data curation, M.G. and E.D.L.; writing—original draft preparation, M.G.; writing—review and editing, M.G., E.D.L. and P.O.; supervision, E.D.L. and P.O.; project administration, P.O.; funding acquisition, P.O. All authors have read and agreed to the published version of the manuscript.

Data Availability Statement: Not applicable.

References

1. Jancovici, J.M.; Blain, C.; Sapin, C. *Le Monde sans Fin*; Dargaud: Paris, France, 2021.
2. Bourmaud, A.; Beaugrand, J.; Shah, D.U.; Placet, V.; Baley, C. Towards the Design of High-Performance Plant Fibre Composites. *Prog. Mater. Sci.* **2018**, *97*, 347–408. [CrossRef]
3. Deshmukh, G.S. Advancement in Hemp Fibre Polymer Composites: A Comprehensive Review. *J. Polym. Eng.* **2022**, *42*, 575–598. [CrossRef]
4. Mudoi, M.P.; Sinha, S.; Parthasarthy, V. Polymer Composite Material with Nettle Fiber Reinforcement: A Review. *Bioresour. Technol. Rep.* **2021**, *16*, 100860. [CrossRef]
5. Richely, E.; Bourmaud, A.; Placet, V.; Guessasma, S.; Beaugrand, J. A Critical Review of the Ultrastructure, Mechanics and Modelling of Flax Fibres and Their Defects. *Prog. Mater. Sci.* **2021**, *124*, 100851. [CrossRef]
6. Placet, V.; Cisse, O.; Boubakar, M.L. Influence of Environmental Relative Humidity on the Tensile and Rotational Behaviour of Hemp Fibres. *J. Mater. Sci.* **2011**, *47*, 3435–3446. [CrossRef]
7. Bourmaud, A.; Pinsard, L.; Guillou, E.; De Luycker, E.; Fazzini, M.; Perrin, J.; Weitkamp, T.; Ouagne, P. Elucidating the Formation of Structural Defects in Flax Fibres through Synchrotron X-ray Phase-Contrast Microtomography. *Ind. Crop. Prod.* **2022**, *184*, 115048. [CrossRef]
8. Quereilhac, D.; Pinsard, L.; Guillou, E.; Fazzini, M.; De Luycker, E.; Bourmaud, A.; Abida, M.; Perrin, J.; Weitkamp, T.; Ouagne, P. Exploiting Synchrotron X-ray Tomography for a Novel Insight into Flax-Fibre Defects Ultrastructure. *Ind. Crop. Prod.* **2023**, *198*, 116655. [CrossRef]
9. Hughes, M. Defects in Natural Fibres: Their Origin, Characteristics and Implications for Natural Fibre-Reinforced Composites. *J. Mater. Sci.* **2011**, *47*, 599–609. [CrossRef]
10. Duc, A.L.; Vergnes, B.; Budtova, T. Polypropylene/Natural Fibres Composites: Analysis of Fibre Dimensions after Compounding and Observations of Fibre Rupture by Rheo-Optics. *Compos. Part A Appl. Sci. Manuf.* **2011**, *42*, 1727–1737. [CrossRef]
11. Beaugrand, J.; Guessasma, S. Scenarios of Crack Propagation in Bast Fibers: Combining Experimental and Finite Element Approaches. *Compos. Struct.* **2015**, *133*, 667–678. [CrossRef]
12. Fuentes, C.A.; Willekens, P.; Hendrikx, N.; Lemmens, B.; Claeys, J.; Croughs, J.; Dupont-Gillain, C.; Seveno, D.; Van Vuure, A. Microstructure and mechanical properties of hemp technical fibres for composite applications by micro computed tomography and digital image correlation. In Proceedings of the 17th European Conference on Composite Materials (ECCM 2016), Munich, Germany, 26–30 June 2016; pp. 26–30.
13. Huguet, E.; Corn, S.; Le Moigne, N.; Ienny, P. Contribution à la caractérisation du comportement mécanique de fibres végétales en environnement contrôlé : fiabilisation d'un banc test de mesure en traction. In Proceedings of the JJC ECOCOMP 2022—5e édition des Journées Jeunes Chercheurs en Eco-composites et Composites Bio-sourcés, Groix, France, 19–21 October 2022.
14. *NF T25-501-2*; Fibres de renfort—Fibres de lin pour composites plastiques—Partie 2: Détermination des propriété s en traction des fibres élémentaires. AFNOR: Paris, France, 2015.
15. *ASTM D3822/D3822M-14*; Standard Test Method for Tensile Properties of Single Textile Fibers. ASTM International: West Conshohocken, PA, USA, 2020. [CrossRef]
16. Garat, W.; Corn, S.; Le Moigne, N.; Beaugrand, J.; Bergeret, A. Analysis of the morphometric variations in natural fibres by automated laser scanning: Towards an efficient and reliable assessment of the cross-sectional area. *Compos. Part A Appl. Sci. Manuf.* **2018**, *108*, 114–123. [CrossRef]
17. Goudenhooft, C.; Bourmaud, A.; Baley, C. Flax (*Linum usitatissimum* L.) Fibers for Composite Reinforcement: Exploring the Link Between Plant Growth, Cell Walls Development, and Fiber Properties. *Front. Plant Sci.* **2019**, *10*, 411. [CrossRef]
18. Del Masto, A.; Trivaudey, F.; Guicheret-Retel, V.; Placet, V.; Boubakar, L. Nonlinear tensile behaviour of elementary hemp fibres: A numerical investigation of the relationships between 3D geometry and tensile behaviour. *J. Mater. Sci.* **2017**, *52*, 6591–6610.
19. Jeannin, T.; Yung, L.; Evon, P.; Labonne, L.; Ouagne, P.; Lecourt, M.; Cazaux, D.; Chalot, M.; Placet, V. Native stinging nettle (Urtica dioica L.) growing spontaneously under short rotation coppice for phytomanagement of trace element contaminated soils: Fibre yield, processability and quality. *Ind. Crop. Prod.* **2020**, *145*, 111997. [CrossRef]
20. Eaton, J.W.; Bateman, D.; Hauberg, S. *Gnu Octave*; Network Thoery: London, UK, 1997.
21. Grégoire, M.; Bar, M.; De Luycker, E.; Musio, S.; Amaducci, S.; Gabrion, X.; Placet, V.; Ouagne, P. Comparing flax and hemp fibres yield and mechanical properties after scutching/hackling processing. *Ind. Crop. Prod.* **2021**, *172*, 114045. [CrossRef]
22. Placet, V.; Trivaudey, F.; Cisse, O.; Gucheret-Retel, V.; Boubakar, M.L. Diameter Dependence of the Apparent Tensile Modulus of Hemp Fibres: A Morphological, Structural or Ultrastructural Effect? *Compos. Part A Appl. Sci. Manuf.* **2012**, *43*, 275–287. [CrossRef]
23. Lefeuvre, A.; Bourmaud, A.; Morvan, C.; Baley, C. Elementary Flax Fibre Tensile Properties: Correlation between Stress–Strain Behaviour and Fibre Composition. *Ind. Crop. Prod.* **2014**, *52*, 762–769. [CrossRef]
24. Duval, A.; Bourmaud, A.; Augier, L.; Baley, C. Influence of the Sampling Area of the Stem on the Mechanical Properties of Hemp Fibers. *Mater. Lett.* **2011**, *65*, 797–800. [CrossRef]
25. Pickering, K.L.; Beckermann, G.W.; Alam, S.N.; Foreman, N.J. Optimising Industrial Hemp Fibre for Composites. *Compos. Part A Appl. Sci. Manuf.* **2007**, *38*, 461–468. [CrossRef]
26. Hughes, T.J.R.; Cottrell, J.A.; Bazilevs, Y. Isogeometric analysis: CAD, finite elements, NURBS, exact geometry and mesh refinement. *Comput. Methods Appl. Mech. Eng.* **2005**, *194*, 4135–4195. .: 10.1016/j.cma.2004.10.008. [CrossRef]

27. Scida, D.; Bourmaud, A.; Baley, C. Influence of the scattering of flax fibres properties on flax/epoxy woven ply stiffness. *Mater. Des.* **2017**, *122*, 136–145. [CrossRef]

28. Haag, K.; Müssig, J. Scatter in tensile properties of flax fibre bundles: Influence of determination and calculation of the cross-sectional area. *J. Mater. Sci.* **2016**, *51*, 7907–7917. [CrossRef]

29. Mattrand, C.; Béakou, A.; Charlet, K. Numerical modeling of the flax fiber morphology variability. *Compos. Part A Appl. Sci. Manuf.* **2014**, *63*, 10–20.

30. Thomason, J.; Carruthers, J. Natural fibre cross sectional area, its variability and effects on the determination of fibre properties. *J. Biobased Mater. Bioenergy* **2012**, *6*, 424–430. [CrossRef]

31. Bourmaud, A.; Shah, D.U.; Beaugrand, J.; Dhakal, H.N. Property Changes in Plant Fibres during the Processing of Bio-Based Composites. *Ind. Crop. Prod.* **2020**, *154*, 112705. [CrossRef]